AIAA JOURNAL
Vol. 36, No. 6, June 1998

Velocimetry and Thermometry of Supersonic Flow Around a Cylindrical Body

Peter F. Barker,* Amberyn M. Thomas,† Timothy J. McIntyre,‡ and Halina Rubinsztein-Dunlop§
University of Queensland, Brisbane, Queensland 4072, Australia

The supersonic flow around a cylindrical body has been studied using two optical techniques. For both sets of measurements, the cylinder was mounted from the side of the tunnel, allowing investigation of the bow shock region as well as in the wake. A new technique, laser-enhanced ionization flow tagging, was used for streamwise velocity determinations behind the body. From these measurements, it was found that the downstream velocity outside the wake was (1.90 ± 0.06) km/s, whereas inside the wake the velocity was about 0–500 m/s in the upstream direction. Planar laser-induced fluorescence of nitric oxide was employed for temperature determinations. It was established that the freestream temperature was (2120 ± 100) K, decreasing to around (1550 ± 400) K in the wake.

Nomenclature

E = energy
$H_{J'J''}$ = Hönl–London factor
I_l = laser pulse energy
J' = rotational quantum number for the lower rotational state of the coupled transition
J'' = rotational quantum number for the upper rotational state of the coupled transition
k = Boltzmann constant
R = ratio of two laser-induced fluorescence signals from different lower rotational levels
T = temperature
ΔE = energy difference between the two lower states

Introduction

OPTICAL techniques have the capability of yielding two-dimensional information in complex supersonic and hypersonic flows. Through the interaction of a laser beam with a given species in the flow, quantities such as rotational and vibrational temperatures,[1,2] densities,[3,4] velocities,[5] and species concentrations[6] have been determined. Such measurements are important in the study of high-speed aerodynamics, for which the conditions can be simulated in a range of shock tunnels and expansion tubes. Recent studies have considered the flow over spheres,[7] cylinders,[8,9] and wedges.[9] Principally, temperature measurements have been used to characterize the conditions in the freestream and behind the bow shock in the flow. Good agreement has been obtained with numerical modeling.

The present study consists of an investigation of a nonreacting supersonic flow around a cylinder. Its purpose is twofold. First, the applicability of a new technique, laser-enhanced ionization (LEI) flow tagging, has been investigated in a complex nonuniform flow. In this method, a laser beam is used to tag a region in the flow by ionizing a selected atomic species, and its motion is monitored by the use of another laser beam fired at a known delay after the first beam. The translation and deformation of the line provides a direct measurement of the streamwise component of the velocity. Second, temperature measurements have been obtained using planar laser-induced fluorescence (PLIF) to provide a more detailed characterization of the flow. In particular, this has focused on the wake region behind the cylinder, which, due to the cylinder's being mounted from the side of the test section, can be examined with minimal outside interference. These measurements provide experimental data that can be used for comparison with computer modeling of the flow. Successful comparison of experimental and numerical studies in a nonreacting flow precedes planned work where both the experimental and numerical techniques will be used to study high-enthalpy, chemically reacting flows.

Presented as Paper 97-0496 at the AIAA 35th Aerospace Sciences Meeting, Reno, NV, Jan. 6–9, 1997; received May 29, 1997; revision received Feb. 12, 1998; accepted for publication Feb. 16, 1998.

*Postdoctoral Research Fellow, Department of Physics.
†Postgraduate Student, Department of Physics.
‡Research Fellow, Department of Physics. Member AIAA.
§Associate Professor, Department of Physics.

Facility

All experiments were performed in a small shock tube called the Drummond tube, shown in Fig. 1. This is a cold-helium-driven facility suitable for generating flows with velocities around 2 km/s. The tube is 4 m long, with a 3.25-m driven section. The driver has a double-diaphragm configuration that consists of two sections, a large reservoir and a smaller reservoir. The purpose of the smaller reservoir is to provide a simple means for firing the shock tube. Aluminum diaphragms were used, which allowed the use of driver pressures of around 4 MPa. The shock tube has a circular cross section with a transition to a square cross section upstream of the test section. It is instrumented with pressure transducers and thin-film temperature gauges for shock speed calculations and timing purposes. The test section is 50 mm square, and three of the four faces are fitted with a quartz window mounted flush with the inside tube surface. The windows have a usable diameter of 20 mm. A 3.7-mm-diam cylinder was sidemounted from the fourth face, which is the face opposite the detection window. Because of this geometry, the region before and after the cylinder was able to be imaged with only minimal interference from the model support. At the end of the shock tube, there is a large dump tank to absorb the expanding driver gas. Table 1 contains the calculated conditions of the flowfield in which these measurements were performed. They are determined from experimental measurements of the shock velocity and initial gas pressure using chemical equilibrium assumptions. The repeatability of the flow in the tunnel is good, with measured velocities deviating by less than 2% from shot to shot.

For velocity measurements, trace amounts of sodium were seeded into an airflow from a second small sodium-coated cylinder placed upstream of the test section. The addition of this small object into the freestream was found not to significantly alter the measured flow speed.[10] The probed species for the PLIF temperature measurements was nitric oxide. Although not produced in an airflow with the moderate-strengthshocks produced in the Drummond tube, nitric oxide is commonly used for diagnostic purposes as it is often present in high-enthalpy airflows and in combusting flows. It is a suitable species for such an investigation because of its relatively well-known spectroscopic constants. In the experiments described here, NO was introduced into the flow by using a test gas with a composition of 5% NO in nitrogen.

Table 1 Conditions expected in the Drummond tube flow assuming chemical equilibrium

	Freestream		Normal shock	
Parameter	Air	5% NO in N_2	Air	5% NO in N_2
Pressure, kPa	89	85	390	330
Temperature, K	2130	2220	2990	3120
Density, kg/m^3	0.15	0.13	0.44	0.36
Enthalpy, MJ/kg	3.7	3.8	3.7	3.8
Velocity, km/s	1.8	1.7	0.56	0.63
Mach number	2.0	1.9	0.53	0.57

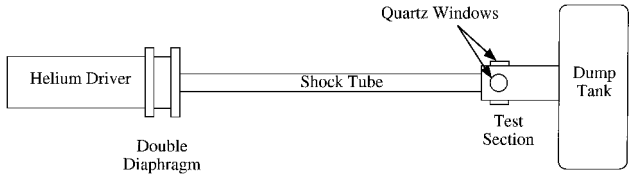

Fig. 1 Schematic diagram of the Drummond tube.

Flow Tagging by LEI

Flow tagging by laser excitation has previously been employed to measure the velocity of a number of high-speed gas flows.[11–13] In these techniques, a well-defined region of the flow is differentiated from its surroundings by creating either a long-lived species or an excited state by laser excitation. The displacement of the tagged region with time is used to calculate a flow velocity. This time-of-flight measurement requires little calibration or detailed knowledge of the flowfield. Tagging in supersonic flows has previously been accomplished by Raman excitation of O_2 (Ref. 11), photodissociation of water and hydrocarbon fuels,[12] and photoionization of UF_6 (Ref. 13). However, these techniques are not readily applicable to the high-temperature air flows produced in our shock tubes, due to either thermal dissociation of the species to be tagged or, in the case of Raman excited O_2, thermal population of the excited state.

Instead, we have developed a technique that generates a tagged region by ionization of atomic sodium that is seeded into or naturally contained in the flow.[10,14] This type of tagging scheme can be applied to a larger variety of flows provided thermal ionization is insufficient to decrease the contrast of the tagged region.

In the tagging scheme presented here, a resonant two-step excitation procedure was employed to tag a region of the flow by selectively promoting ground state sodium atoms in a small region to an excited state close to the ionization limit. Following laser excitation, efficient ionization occurs when the excited sodium atoms gain a total energy greater than that required for ionization through inelastic collisions with surrounding molecules. Figure 2a is a diagram presenting the two-step LEI process employed to tag sodium in the flow. In the first step of this excitation scheme, a laser pumps atoms from the ground electronic state to an intermediate excited state ($3p_{3/2}$) using light at a wavelength of 589 nm. Immediately, a second laser pumps atoms from the intermediate excited state to the $7d$ state that is approximately 0.2 eV below the ionization limit. For this second step, light at a wavelength of 449 nm was employed. Collisions then serve to ionize approximately 80% of the irradiated atoms in the duration of the laser pulse.[14] To detect the tagged region, PLIF of the neutral sodium was performed and the tagged region was observed as a reduction in the signal in the PLIF image. Thus, the ionized tagged region was seen as a hole in the otherwise bright background of the neutral sodium fluorescence. Figure 2b is a diagram representing the LIF excitation scheme used to detect the tagged region.

Optical Arrangement for Flow Tagging in the Shock Tube

The two laser beams required for the two-step LEI process were provided by a two-color dye laser system constructed in-house. The combined two-wavelength output of this system is termed the *depleting beam.* A third dye laser was used as the probe laser to detect the depleted ground state of sodium by exciting the remaining ground state atoms to the $3p_{3/2}$ state and monitoring the resonance fluorescence at 589 nm.

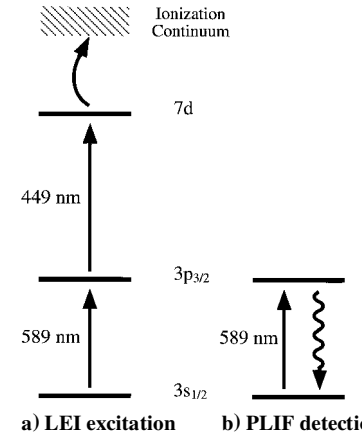

Fig. 2 Excitation and detection scheme for velocimetry.

Prior to performing velocity measurements in the shock tube, the depleting lasers and the probe laser were tuned to the absorption line center of the transitions by using an air/acetylene flame seeded with sodium. In this procedure, the first-step LEI laser and the probe laser were tuned so that maximum fluorescence was observed from the $3s_{1/2}$–$3p_{3/2}$ transition in sodium. With the first-step laser fixed at this frequency, the second-step laser was tuned while monitoring the resonance fluorescence from the first excitation step ($3s_{1/2}$–$3p_{3/2}$). Line center operation for the second step was determined when a minimum in the fluorescence signal was detected. This indicated maximum transferral of atoms to the ionized state via the upper state of the second excitation step.

For measurements in the shock tube, the depleting and probe laser beams were directed through the top and bottom windows of the test section, respectively. These two counterpropagating beams were expanded into thin sheets of light approximately 2 mm thick, and the sheets were oriented at right angles to each other. Both the depleting beam and the probe beam were shaped by a combination of spherical and cylindrical lenses. In this simple beam shaping scheme, a spherical lens is used to form a focus at the center of the test section, while the cylindrical lens diverges the light in only one plane to form a diverging sheet of light. A spherical lens of +500-mm focal length was used in both the tagging and probe beam shaping optics. For the depleting beams, a cylindrical lens of +50-mm focal length was employed to expand the beam to a sheet approximately 8 mm wide, with its width perpendicular to the flow direction. A cylindrical lens of focal length +25 mm was employed to expand the probe beam to a larger width of approximately 25 mm. The 25-mm width of the excitation sheet was chosen to fill the field of view of the windows and was aligned to be parallel with the tube flow. A depleting beam shape in the form of a sheet was employed to limit the transport of untagged flow into the tagged region, where the depletion and probe sheets intersect. Transport of neutral sodium into this region has the effect of reducing the contrast and, hence, the visibility of the tagged region. This planar shape also acts to maintain tagged line visibility when the probe sheet is skewed at some angle away from the flow. In this case, displacement of the tagged region out of the plane of the probe sheet can occur when the width of the tagging beam is not much greater than the thickness of the probe sheet.

The orientation of the detection optics and equipment around the test section is shown in Fig. 3. In this arrangement, one of the side windows was used to monitor the convection of the tagged flow. A $f/4.5$ uv Nikkor lens was placed outside this window to collect and image the planar LIF signal from the untagged sodium atoms in the flow. This image was detected by an intensified charge-coupled device (CCD) camera (Princeton Instruments ICCD-576) and subsequently stored in the computer. A Schott glass OG-550 cutoff filter was placed before the lens to allow only fluorescence at 589 nm to be transmitted, thereby removing any scattered blue light at 449 nm from the tagging beam. Although scattered light at 589 nm could not be removed, interference from this source was found to be small compared with the measured LIF signals. The final precise alignment of the depletion and probe beams was accomplished by

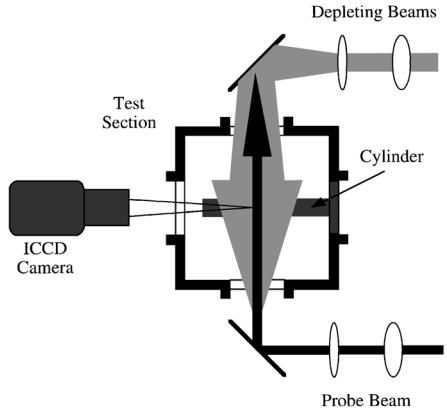

Fig. 3 Optical arrangement around the shock tube test section for velocimetry.

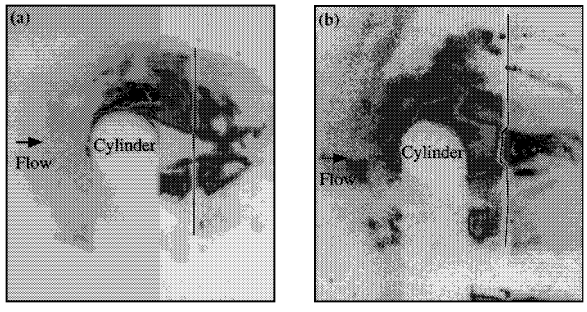

Fig. 4 PLIF images of the tagged flow, tagged region highlighted by dark line, flow left to right, at creation probe delays of a) 40 and b) 176 ns

introducing a small, sodium seeded, butane flame into the test section. Good overlap of the laser beams within the test section was indicated by detecting, with the ICCD camera, a line of depletion in the otherwise uniform fluorescence field created by the probe beam.

Velocity Measurements in the Wake of a Cylindrical Body

Prior to measurements of the velocity in the wake of the cylindrical body, the freestream velocity was measured by performing LEI flow tagging velocimetry. These results were in agreement with the velocity determined from shock speed measurements.[10] Flow tagging velocity measurements were then performed in the wake of a cylindrical body placed in the seeded freestream flow by measuring the streamwise velocity at various locations across the flow.

Figures 4a and 4b are images of the flow behind the cylindrical body containing the depleted tagged region. They correspond to a depletion-probedelay of 40 and 176 ns, respectively. Although these two images were taken in two consecutive shots, presuming shot-to-shot reproducibility, they show the displacement of the tagged region that would occur in a time interval of 136 ns in one shot. The light circular region in each image is the outline of the cylindrical body. The shadow of this cylinder extends to the bottom of the page and is produced by the probe laser sheet directed toward the bottom of the page. A difficulty encountered during the experiment was obtaining uniform seeding of sodium into the flow. As can be seen, the fluorescence signal is very nonuniform. Nevertheless, the depleted regions are easily identifiable in the raw images and are here shown with a dark line to emphasize their location. The nonuniform seeding is, therefore, not seen as a major drawback to the technique, although a method for more uniform seeding would be desirable.

Figure 5 is a plot of the position of the tagged lines in the wake of the cylindrical body for four creation-probe delays. The outer portions of the flow show a smooth evolution with time and can be used to determine the streamwise component of velocity. Immediately behind the cylinder, the velocity is much lower, and in places the gas is seen to move in an upstream direction. There is a strong velocity shear between these two regions. The curve for a delay of 580 ns illustrates a problem that occurred during the measurements.

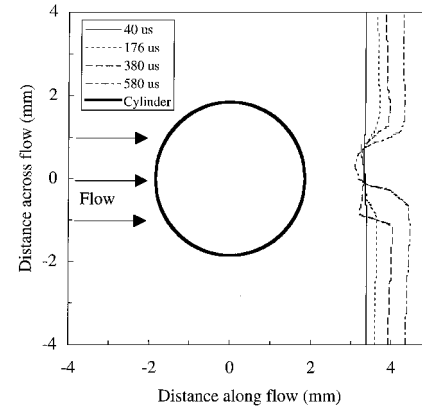

Fig. 5 Position of the center of the tagged line for four creation probe delays.

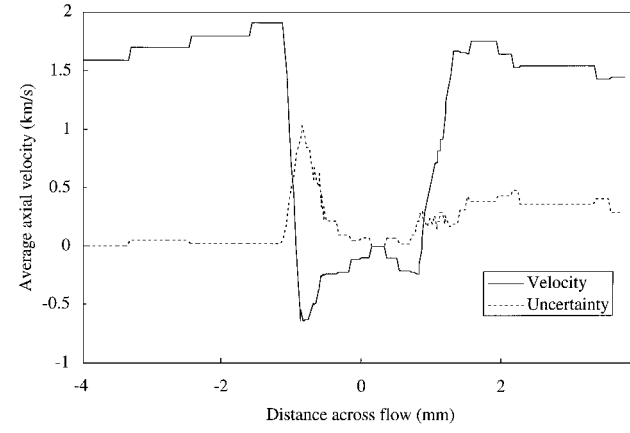

Fig. 6 Measured average streamwise velocity across the flow 2 mm behind the cylinder.

As is seen, the velocity distribution is not symmetrical about the cylinder. It appears as if the freestream velocity was not axial along the tube. Inspection of the original images shows that there is some variation in the location of the wake. One possible explanation is that the method of seeding sodium into the flow (by the introduction of a coated object into the flow upstream of the cylinder) is also causing flow disturbances. This could be eliminated by developing a better seeding method or moving the object farther upstream.

The average streamwise velocity was calculated by using the images with delays of 40, 176, and 380 ns (the 580-ns image was discarded because of the asymmetry). For each position across the flow, the axial position of the tagged region at each delay was determined and a velocity obtained by a linear fit. Figure 6 shows this velocity distribution. Away from the cylinder, the velocity is about 1.6 km/s. The flow is seen to accelerate as it passes around the cylinder, reaching a maximum velocity of (1.90 ± 0.06) km/s just outside the shear layer. Within the wake, the velocity lies between 0 and 500 m/s in an upstream direction. The uncertainty in the fit is also shown in Fig. 6. The largest uncertainties are in the shear layer itself. In this region the average measured velocity is not a true representation of the flow as the velocity varies greatly during the time of the measurements. To obtain the total velocity (as opposed to the streamwise velocity) in nonuniform regions, the flow must be tagged with a mesh of points instead of lines. This could be implemented using the two-step LEI flow tagging technique but was not investigated here due to the small size of the optical access windows. The method is currently under investigation.

PLIF Thermometry

PLIF is a species-specific, nonintrusive diagnostic technique that has found application for a variety of flow and combustion studies.[15,16] In PLIF, a laser that is tuned to a transition of a species of interest is formed into a sheet and passed through a flow. A fraction of the subsequent fluorescence can be collected at 90 deg to

the interaction plane, and this plane can be imaged onto a sensitive two-dimensional detector, yielding a spatially resolved PLIF image. Using a pulsed laser with a pulse duration of the order of 10 ns, high-temporal resolution is achievable, even in very fast flows. With certain limitations, it is possible to determine a two-dimensional temperature map by using two PLIF images resulting from exciting transitions within the same molecular band.[16] This is because a PLIF image contains information about the population of the probed species in the lower state of the transition, which is related to temperature via the Boltzmann distribution. It has been successfully demonstrated for determinations of important physical parameters in supersonic flows, including temperature and velocity.[16] PLIF thermometry of nitric oxide has been employed for both rotational and vibrational temperature measurements by judicious selection of lower energy levels in shock tube and tunnel flows.[1,2,8,9] In this paper, PLIF thermometry of NO is employed for rotational temperature determinations in the supersonic flowfield around a cylinder placed in the Drummond tube. The two-dimensional temperature field obtained includes the region behind the cylinder.

PLIF thermometry theory is well established, and it will not be presented in detail here. It can be shown under certain circumstances that the ratio R of two temporally integrated linear LIF signals resulting from the excitation of transitions originating in different lower rotational levels of the same vibrational level and promoted via laser absorption to the same upper vibrational level can be used to obtain the following expression for the temperature of the flow[16]:

$$T = (-\Delta E) \Big/ k\ell n\left(\frac{R^* I_{L2}{}^* H_{J'J''2}}{I_{L1}{}^* H_{J'J''1}}\right) \tag{1}$$

where ΔE is the difference in the energies of the lower states of the laser coupled transition, I_{L1} and I_{L2} are the laser pulse energies for each excitation, and $H_{J'}$ and $H_{J''}$ are the Hönl–London factors for the transitions.

In reducing the expressions for the two fluorescence signals to the expression from which the temperature is calculated, certain assumptions must be made. The transitions chosen for excitation must be free from spectral interference from neighboring lines, as well as from other species. The spectral overlap of the laser and absorption line shapes must also be the same for both PLIF images. The fluorescence yield must be the same for both transitions. For the $A^2\Sigma^+$ state of nitric oxide, the total quenching rate coefficient and the radiative lifetime is J' independent, so that this criterion is satisfied.[17–19] To eliminate the problems of laser beam attenuation, the strength of the transitions for excitation is a consideration. The laser spectral intensity must be such that the fluorescence is in the linear regime to avoid saturation effects. Ideally, the energy level separation of the two lower levels should be approximately equal to the temperature of the flow to ensure good temperature sensitivity.

Experimental Arrangement for PLIF

The experimental arrangement for PLIF thermometry is shown in Fig. 7a. There are three distinct parts: the laser system, the beam profile monitoring system, and the image detection system. The exciting laser was the frequency-doubled output of a Nd:YAG pumped dye laser operating with the dye coumarin 47. The pulse energy was approximately 500 μJ at 226 nm, and a fraction of this was used in the laser sheet ($\sim$100 μJ). The 226-nm light was focused using a cylindrical lens (ℓ = 30 mm) and a spherical lens (ℓ = 500 mm) to a sheet 500 μm $\times$ 2 cm in the test section. To perform laser sheet energy corrections to the PLIF images, a beam profile monitoring system was employed. Before the test section, a quartz plate redirected a fraction of the laser sheet to a dye cell containing a very strong solution of rhodamine B, which fluoresced under 226-nm excitation. This visible fluorescence, which represented the beam profile, was imaged with an Electrim EDC-1000 CCD camera. A Princeton Instruments ICCD camera fitted with a Nikkor quartz lens (ℓ = 104 mm) was used for detecting the PLIF signal. A Schott glass UG5 filter was placed before the ICCD to reject scattered laser light. This filter also served to eliminate possible problems due to radiation trapping as the filter rejects fluorescence in the (0, 0) vibrational band. The form of the image is shown in Fig. 7b.

Table 2 Transitions, Hönl–London factors, and lower-state energy levels

Transition	Hönl–London factor	Energy of J'' level, cm^{-1}
$P_2 + {}^PQ_{12}(8)$	2.968	229.756
$P_1(29)$	6.1836	1503.299
$P_2 + {}^PQ_{12}(39)$	11.201	2714.978

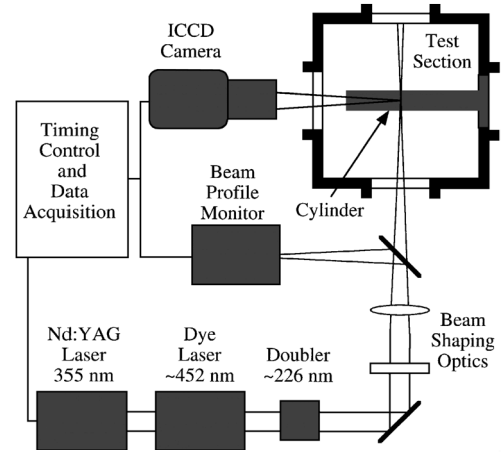

Fig. 7a PLIF arrangement.

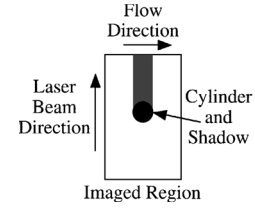

Fig. 7b Imaged region.

The experimental system consists of a one-laser, one-camera system, so that it is possible to obtain only a single PLIF image, from exciting one transition, during each shock tube run. To obtain temperature it is, therefore, necessary to record images in successive shock tube runs and assume flow reproducibility. In multiple shot measurements, the collection optics efficiency is assumed not to change during the course of the experiments. Both the beam profile monitoring system camera and the ICCD camera were operated in their linear regimes.

To maximize signal to noise in the temperature measurements, the energy difference between the lower levels of the two selected transitions should be approximately equal to kT, where T is the anticipated temperature of the flow. In a flow where the temperature has a wide range of values, good sensitivity over the entire range can best be obtained by employing a range of lower states. For this work, the three lines $P_2 + {}^PQ_{12}(8)$, $P_1(29)$, and $P_2 + {}^PQ_{12}(39)$ in the $A^2\Sigma^+ - X^2\Pi(0,0)$ band of nitric oxide were excited. As well as providing good signals for the wide temperature range expected, these lines were chosen because they are free from spectral interference from neighboring lines. The Hönl–London factors have been calculated from the expressions given in the literature[20] and are quoted together with the energies of the lower states in Table 2.

Prior to performing measurements in the shock tube, the lines were investigated and identified in an air/acetylene flame. Figure 8 shows an excitation scan around the $P_1(29)$ transition. Similar scans were obtained for the other lines. This system was later used for tuning the laser immediately prior to a shock tube run.

Thermometry Results

Raw images and beam profiles were obtained for the three lines at the conditions given in Table 1. Example single-shot images for the different excitations are presented in Fig. 9. They show flow from left to right over the cylinder with the laser sheet propagating

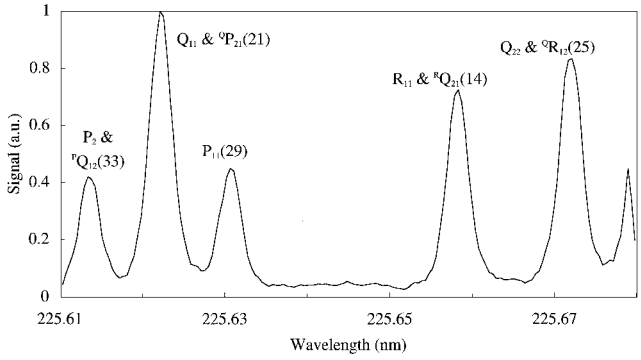

Fig. 8 Excitation scan in an air/acetylene flame around the $P_{11}(29)$ transition; NO lines in this region are identified and labeled.

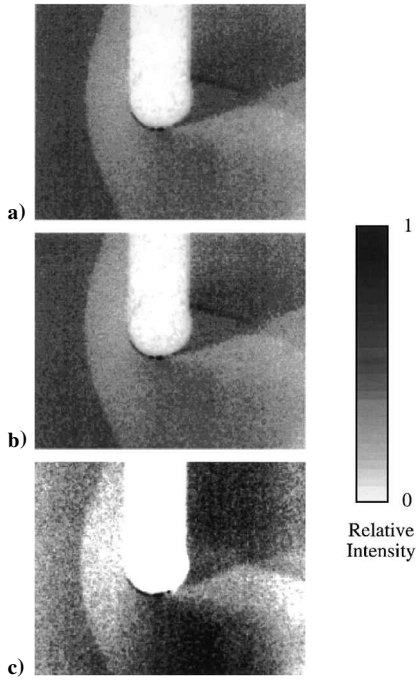

Fig. 9 Single-shot raw images of the flow (left to right) over a cylinder; the excited transitions are a) $P_2 + {}^{P}Q_{12}(8)$, b) $P_1(29)$, and c) $P_2 + {}^{P}Q_{12}(39)$.

from bottom to top. (The shadow of the cylinder can be seen at the top of the images.) In each case, the shock wave is clearly evident, as well as structure in the wake of the body. The signals in these images were very repeatable with no evidence of unsteadiness in the flow being observed. This is in contrast to the LEI images, where the direction of the wake was observed to vary from shot to shot. This lends support to the explanation that the unsteadiness in the LEI measurements was due to the influence of the body upstream of the cylinder used to seed sodium into the flow rather than some inherent unsteadiness of the flow over the cylinder, as has been observed elsewhere.[8] Also note that the uniformity of the signal in the freestream indicates that there is no significant laser absorption across the image.

The raw single-shot images were corrected for camera background, as well as for the laser beam profile, and then normalized by the Hönl–London factor for the particular transition. The corrected images were then averaged and the intensity ratios determined for each pixel in the images. Equation (1) was then evoked to obtain a temperature map of the flow. With the three lines, $P_2 + {}^{P}Q_{12}(8)$, $P_1(29)$, and $P_2 + {}^{P}Q_{12}(39)$, it is possible to determine the temperature using three different ratios. The temperature maps obtained using these ratios are shown in Fig. 10. These temperature maps were obtained using averages of five images for each line except for the $P_2 + {}^{P}Q_{12}(39)$ line in which six were used. Figures 10a, 10b, and 10c show the temperature maps for ratios of the lines

Table 3 Experimentally measured temperatures, degrees Kelvin

Line ratio	Freestream	Bow shock	Wake
29/39	2040	2880	1350
8/29	2200	3140	1770
8/39	2110	3000	1540
Average	2120	3000	1550

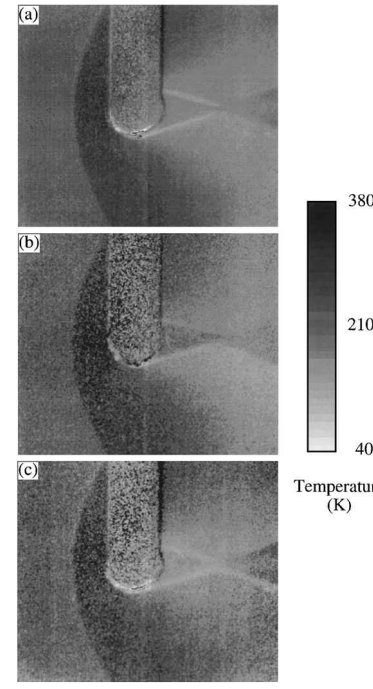

Fig. 10 Temperature maps determined using ratios of images; flow is from left to right. The excited transitions are a) $P_2 + {}^{P}Q_{12}(8)$ and $P_2 + {}^{P}Q_{12}(39)$, b) $P_2 + {}^{P}Q_{12}(8)$ and $P_1(29)$, and c) $P_1(29)$ and $P_2 + {}^{P}Q_{12}(39)$.

$P_2 + {}^{P}Q_{12}(8)$ and $P_2 + {}^{P}Q_{12}(39)$, $P_2 + {}^{P}Q_{12}(8)$ and $P_1(29)$, and $P_1(29)$ and $P_2 + {}^{P}Q_{12}(39)$, respectively. These temperature maps compare well to each other and reflect the expected temperature variation around the model. Of particular interest are the temperature measurements in the wake of the body and the visualization of shear layers and shock waves. The wake is significantly cooler than the freestream due to convective heat loss to the surface of the cylinder.

There is some variation in the determined temperature maps, particularly behind the shock and inside the wake. Table 3 lists the temperature obtained using the three different ratios in different areas of the flow. The freestream temperature is consistent between the images. Averaging the data for the three ratios yields a freestream temperature of (2120 ± 100) K, compared with the calculated value of 2220 K in Table 1. The uncertainties quoted are estimated from inspection of variations in each of the three temperature profiles.

The temperatures obtained in the shock-heated region are less consistent than in the freestream. The average of the three measurements yields a temperature of (3000 ± 200) K, which is in agreement with the predicted value of 3120 K shown in Table 1. This region is characterized by high pressures (above 300 kPa), so that broadening could lead to errors in the determined temperatures because transitions in the wings of the chosen lines may contribute to the PLIF signal. This would be most significant for the $P_1(29)$ line because it is a relatively weak line and has a strong neighboring line $[Q_{11} + {}^{Q}P_{21}(21)]$. It would be expected, therefore, that the ratios of $P_2(8)$ and $P_1(29)$ and $P_1(29)$ and $P_2(39)$ would be the most affected by this influence of neighboring lines. In this shock-heated region, where quenching is significant, the population reduction of lower J'' levels may cause increased uncertainty in the temperature maps determined using lines originating from less populated levels, i.e. $P_2(8)$. Another important consideration in this region is the constancy of the fluorescence yield, which for these determinations we have assumed is J' independent. This assumption is

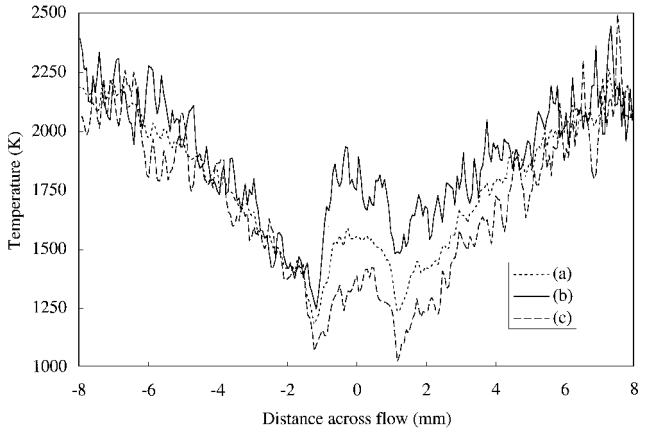

Fig. 11 Temperature profile across the flow 1 mm behind the cylinder. The excited transitions are a) $P_2 + {}^PQ_{12}(8)$ and $P_2 + {}^PQ_{12}(39)$, b) $P_2 + {}^PQ_{12}(8)$ and $P_1(29)$, and c) $P_1(29)$ and $P_2 + {}^PQ_{12}(39)$.

based on previous studies in which high J' levels have not been investigated.[18–20]

Figure 11 shows cross sections of the temperature maps taken approximately 1 mm behind the cylinder across the wake. The temperature profile is seen to decrease from the freestream value of 2120 K to a temperature of 1400 K just outside the shear layer. The cross sections obtained from the different line pair ratios in the regions outside the wake compare reasonably well. Between the shear layers, inside the wake, the agreement for the different line pairs is poor. The average temperature obtained in this region using data from all three line pairs is (1550 ± 400) K. In the wake, where significant cooling has occurred due to convective heat transfer, the population reduction of higher J'' levels may cause increased uncertainty in the temperature profiles. The variation in the determined temperatures in this region could also be attributed to saturation effects, which may become important because of the lower pressures in this region. Other possibilities for the discrepancy in this region are nonequilibrium effects and flow unsteadiness. An investigation of the flowfield using computational fluid dynamics codes (CFD) is currently in progress, and this will be used to further analyze the temperature field. Emphasis will be placed on determining the cause for the temperature variations obtained in the wake of the cylinder. The results in other regions of the flow, for which the agreement between temperatures obtained using different line pairs is good, provide experimental measurements that can be compared with future calculations of the flow to facilitate important CFD model validation.

Summary and Conclusion

The LEI flow tagging technique was successfully applied to the measurement of velocities in the wake of a cylindrical body. The experimental arrangement employed to achieve flow tagging in the shock tube flow was described, and velocity measurements behind a cylindrical body placed in the freestream flow were presented. From these measurements, it was found that the downstream velocity outside the wake was (1.90 ± 0.06) km/s, whereas inside the wake the velocity was in the range 0–500 m/s in the upstream direction.

Temperature maps of the flow around a cylinder were obtained using PLIF thermometry of nitric oxide. The temperature profiles obtained using different transition pairs compare well in the freestream, yielding a freestream temperature of (2120 ± 100) K. Behind the model, the temperature was seen to decrease from the freestream temperature to around (1550 ± 400) K in the wake inside the shear layers. There is variation in the temperature fields obtained in some regions of the flow, particularly in the wake of the cylinder, which may be due to saturation or nonequilibrium effects. This is the subject of a current study that aims to investigate the properties of the flow using CFD codes.

Acknowledgments

This work was supported by the Australian Research Council. The authors gratefully acknowledge the contribution of Alexis Bishop. Assistance from the workshops in the Department of Physics and the Department of Mechanical Engineering is also acknowledged.

References

[1] McMillin, B. K., Palmer, J. L., and Hanson, R. K., "Temporally Resolved, Two-Line Fluorescence Imaging of NO Temperature in a Transverse Jet in Supersonic Cross Flow," *Applied Optics*, Vol. 32, No. 31, 1993, p. 7532.

[2] Palmer, J. L., and Hanson, R. K., "Planar Laser-Induced Fluorescence Imaging in Free Jet Flows with Vibrational Non-Equilibrium," AIAA Paper 93-0046, Jan. 1993.

[3] McIntyre, T. J., Wegener, M. J., Bishop, A. I., and Rubinsztein-Dunlop, H., "Simultaneous Two-Wavelength Holographic Interferometry in a Superorbital Expansion Tube Facility," *Applied Optics*, Vol. 36, No. 31, 1997, pp. 8128–8134.

[4] Kastell, D., Carl, M., and Eitelberg, G., "Phase Step Holographic Interferometry Applied to Hypervelocity, Non-Equilibrium Cylinder Flow," *Experiments in Fluids*, Vol. 22, No. 1, 1996, pp. 57–66.

[5] Paul, P. H., Lee, M. P., and Hanson, R. K., "Molecular Velocity Imaging of Supersonic Flows Using Pulsed Planar Laser-Induced Fluorescence of NO," *Optics Letters*, Vol. 14, 1989, pp. 417–419.

[6] Abbitt, J. D., III, Hartfield, R. J., and McDaniel, J. C., Jr., "Mole-Fraction Imaging of Transverse Injection in a Ducted Supersonic Flow," *AIAA Journal*, Vol. 29, No. 3, 1991, pp. 431–435.

[7] Allen, M. G., Cronin, J. F., Davis, S. J., Foutter, R. R., Parker, T. E., Reinecke, W. G., and Sonnefroh, D. M., "PLIF Imaging Measurements Compared to Model Calculations in High Temperature Mach 3 Airflow Over a Sphere," AIAA Paper 93-0092, Jan. 1993.

[8] Houwing, A. F. P., Palmer, J. L., Thurber, M. C., Wehe, S. D., Hanson, R. K., and Boyce, R. R., "Comparison of Planar Fluorescence Measurements and Computational Modeling of Shock-Layer Flow," *AIAA Journal*, Vol. 34, No. 3, 1996, pp. 470–477.

[9] Palma, P. C., McIntyre, T. J., and Houwing, A. F. P., "PLIF Imaging in Shock Tunnel Flows Using a Raman-Shifted Tunable Excimer Laser," *Shock Waves* (to be published).

[10] Barker, P., Bishop, A., and Rubinsztein-Dunlop, H., "Supersonic Velocimetry Using Laser Enhanced Ionisation and Planar Laser Induced Fluorescence," *Applied Physics B*, Vol. 64, No. 3, 1997, pp. 369–376.

[11] Miles, R. B., Connors, J. J., Markovitz, E. C., Howard, P. J., and Roth, G. J., "Instantaneous Profiles and Turbulence Statistics of Supersonic Free Shear Layers by Raman Excitation Plus Laser-Induced Electronic Fluorescence (RELIEF) Velocity Tagging of Oxygen," *Experiments in Fluids*, Vol. 8, 1989, p. 17.

[12] Boedecker, L. R., "Velocity Measurement by H_2O Photolysis and Laser-Induced Fluorescence of OH," *Optics Letters*, Vol. 14, No. 10, 1989, p. 473.

[13] Krauss, R., Popp, C., and Scott, J., "Countercurrent Velocity Measurements in a Rotating Frame of Reference," *Bulletin of the American Physical Society*, Vol. 32, No. 10, 1987, p. 2095.

[14] Barker, P., Thomas, A., Ljungberg, P., and Rubinsztein-Dunlop, H., "Velocity Measurements by Flow Tagging Employing Laser Enhanced Ionisation and Laser Induced Fluorescence," *Spectrochimica Acta B*, Vol. 50, 1995, p. 1301.

[15] Eckbreth, A. C., *Laser Diagnostics for Combustion Temperature and Species*, Abacus, Cambridge, MA, 1988.

[16] Palmer, J. L., McMillan, B. K., and Hanson, R. K., "Planar Laser-Induced Fluorescence Imaging of Velocity and Temperature in Shock Tunnel Free Jet Flow," AIAA Paper 92-0762, Jan. 1992.

[17] McDermid, I. S., and Laudenslager, J. B., "Radiative Lifetimes and Electronic Quenching Rate Constants for Single-Photon-Excited Rotational Levels of NO ($A^2\Sigma^+$, $v' = 0$)," *Journal of Quantitative Spectroscopy and Radiation Transfer*, Vol. 27, No. 5, 1982, pp. 483–492.

[18] Nutt, G. F., Haydon, S. C., and McIntosh, A. I., "Measurement of Electronic Quenching Rates in Nitric Oxide Using Two-Photon Spectroscopy," *Chemical Physics Letters*, Vol. 62, No. 2, 1979, pp. 402–404.

[19] McGee, T. J., Miller, G. E., Burris, J., Jr., and McIlrath, T. J., "Fluorescence Branching Ratios from the $A^2\Sigma^+(v' = 0)$ State of NO," *Journal of Quantitative Spectroscopy and Radiation Transfer*, Vol. 29, No. 4, 1983, pp. 333–338.

[20] Earls, L. T., "Intensities in $^2\Pi$-$^2\Sigma$ Transitions in Diatomic Molecules," *Physics Review*, Vol. 48, Sept. 1935, pp. 423, 424.

G. Laufer
Associate Editor